NANO LETTERS

2006
Vol. 6, No. 12
2773−2780

Observation of Superconductivity in Granular Bi Nanowires Fabricated by Electrodeposition

Mingliang Tian,*[,†,‡] Jinguo Wang,[†,§] Nitesh Kumar,[†,‡] Tianheng Han,[†,∥] Yoji Kobayashi,[⊥] Ying Liu,[‡] Thomas E. Mallouk,*[,†,‡,⊥] and Moses H. W. Chan*[,†,‡]

Center for Nanoscale Science (CNS), Department of Physics, Department of Chemistry, and Materials Research Institute (MRI), Pennsylvania State University, University Park, Pennsylvania 16802-6300, and Department of Physics, the Hong Kong University of Science and Technology, Clear Water Bay, Hong Kong, People's Republic of China

Received August 2, 2006; Revised Manuscript Received October 26, 2006

ABSTRACT

Bulk rhombohedral Bi at ambient pressure is a well-known semimetal, and its transition to a superconductor has not been observed, at least down to 50 mK. We report that, unlike bulk rhombohedral Bi, granular Bi nanowires with well-defined rhombohedral grains of ~10 nm diameter, fabricated by electrochemically depositing Bi into porous polycarbonate membranes at ambient pressure, are superconducting with two transition temperatures, T_c, of 7.2 and 8.3 K. These T_c values coincide with T_c values of the high-pressure phases Bi–III and Bi–V, respectively. Analysis of our structural and transport data indicates that the superconductivity in granular Bi nanowires probably arises from grain boundary areas where there are structural reconstructions between the grains showing a preferred orientation within a small angular distribution.

It is well-known that bulk rhombohedral Bi at ambient pressure is not a superconductor down to 50 mK.[1] Unlike other materials, rhombohedral Bi can be a metal, semimetal, and semiconductor. Its electronic properties depend sensitively on the sample size and geometry (bulk,[1,2] films,[3,4] cylinder or filament,[5] nanowires,[6−10] or tubes[11]), quality (defects or impurity), and morphology (single-crystal,[1−6] polycrystal[4,8] or granular[9]). Because of its unusually rich electronic properties, Bi has long been the subject of experimental and theoretical studies.[1−11]

At high pressure, however, Bi is superconducting at low temperatures due to the formation of high-pressure metallic polymorphs, namely, monoclinic Bi−II at 2.55 GPa,[12,13] a complex tetragonal Bi−III at 2.7 GPa,[12,14−16] and a body-centered cubic (bcc) Bi−V at 7.7 GPa.[12,16,17] The transition temperatures of these polymorphic phases are respectively 3.9,[18,19] 7.2,[18−20] and 8.3 K.[20,21] It was found that these high-pressure phases could be preserved in a metastable state by subjecting the bulk crystal to compression cycles at room temperature and releasing the pressure at helium temperatures.[20] When the samples are annealed at a temperature higher than 20 K, the metastable high-pressure phases disappear. In these compression cycles, internal microstresses are usually formed as a result of plastic deformation due to an increase in the number of dislocations and a greater degree of polycrystallinity.[20] At ambient pressure, Bi can be superconducting under three specific conditions: (1) Bi amorphous film with disorder on the atomic scale, fabricated by condensing Bi onto a liquid helium cooled substrate. The T_c is around 6.0 K.[22] (2) Bi granular composite films, fabricated by codepositing Bi and matrix gas (A = Kr, Xe, O_2, and H_2) onto cold substrates at $T < 40$ K. These composite films consist of rhombohedral Bi grains surrounded by insulating solid matrix gas with a concentration ratio of Bi:A = x:(1 − x) with $x \sim 0.34-0.89$.[23,24] The transition temperature, which is generally below 5.5 K, is strongly grain size dependent and is influenced by the surrounding solid matrix. Without the solid gas matrix, a pure Bi granular film is not superconducting. The superconducting property in these granular Bi composite films was initially interpreted by Weitzel and Micklitz[23] as a quantum size effect due to a strongly enhanced density of states at the Bi grain surface. However, Vossloh, Holdenried, and Micklitz[25] presented new data that indicated that the superconductivity in Bi granular composite films is not related to the quantum size effect. They speculated that the original

* Corresponding authors. E-mail address: mut1@psu.edu (Tian), tom@chem.psu.edu (Tom), and chan@phys.psu.edu (Chan).
† Center for Nanoscale Science (CNS), Pennsylvania State University.
‡ Department of Physics, Pennsylvania State University.
§ Materials Research Institute (MRI), Pennsylvania State University.
∥ Department of Physics, the Hong Kong University of Science and Technology.
⊥ Department of Chemistry, Pennsylvania State University.

10.1021/nl0618041 CCC: $33.50
Published on Web 11/10/2006

rhombohedral structure of Bi grains might become progressively distorted (with higher density of defects) with decreasing grain size until the Bi grains change into an "amorphous" structure at a grain size of about 4.0 nm. (3) Bi film on a thin Ni film substrate (1−4 nm of Ni/40−70 nm of Bi bilayer).[26,27] The T_c is around 4.0 K, and the superconductivity was thought to originate from the stress between Bi and Ni layers which induces a face-centered cubic structure of the Bi film (this phase does not survive in bulk Bi or Bi film without a Ni layer) or a common rhombohedral phase with a (102) preferred orientation.[28]

In this paper we report the observation of superconductivity in granular Bi nanowires, fabricated by electrochemical deposition at room temperature and measured at ambient pressure. The superconductivity is subtle, in that the nanowires can be superconducting or non-superconducting, sensitively depending on the details of sample morphology. We investigated 38 granular Bi nanowire samples fabricated with the same technique; 18 of them showed superconductivity at low temperatures. Transmission electron microscopy (TEM) study showed that the superconducting Bi nanowires have a uniform granular morphology with all the rhombohedral Bi grains (∼10 nm) aligned with a preferred orientation along the entire length of the wire. Two superconducting transitions, one at 8.3 K with a large and sharp resistance drop and another one at 7.2 K with a smaller resistance drop, were seen. Both transition temperatures are higher than those reported for amorphous Bi film, granular Bi composite films, and Bi/Ni bilayers but coincide with the T_c values of high-pressure phases Bi−III and −V.[20,21] For the non-superconducting granular Bi samples, the rhombohedral Bi grains show random orientation and both wire diameter and the grain size also show considerable variations along the length of the wire. Because the transport properties depend sensitively on the sample morphology, TEM images were always obtained on the same sample after each transport measurement. Our observation of different structural morphologies in superconducting and non-superconducting granular Bi nanowires suggests that the superconductivity is not from the size confinement effect of the rhombohedral Bi grains but probably arises from small amounts of high-pressure phases formed at the boundaries between the partially aligned grains.

Bismuth nanowires used in this work were fabricated by electrochemically depositing Bi into porous polycarbonate (PC) membranes at room temperature. One of the advantages of this technique is that the morphology of the fabricated nanowires can be controlled to a large extend by selecting appropriate additives, pH, deposition potential, and temperature.[29] The Bi electrolyte was prepared by the following procedure. (i) 6.2 g of H_3BO_3, 15.0 g of tartaric acid, 13 mL of glycerol, and 6.0 g of gelatin were added in succession to 300 mL of distilled water at room temperature, followed by sonication for 10 min in an ultrasonic bath. (ii) 5.84 g of NaCl, 8.7 g of K_2SO_4, and 2.43 g of $Bi(NO_3)_3 \cdot 5H_2O$ were added, the solution was stirred for 1 min in the ultrasonic bath (the solution became milky white), and then the solution was made clear by adding 22 mL of concentrated HNO_3. (iii) The solution was diluted with distilled water up to total volume of 500 mL. A pure Pt wire was used as the positive electrode, and Au film evaporated on one side of the membrane prior to electrodeposition was used as the negative electrode. Electrodeposition was done using a two-electrode system (the distance between two electrodes was kept at 3.0 cm) at room temperature with a dc voltage between −2.2 and −3.0 V. NaCl, K_2SO_4, and gelatin work as additives to control the grain size, promote ion transfer, and improve the wettability. Without these additives, the solution still works for Bi growth, but large grains or single-crystalline segments result. The diameter and length of the nanowires are controlled by the pore size and the thickness of the template, but the actual diameter of the resultant nanowires is usually several times larger than the quoted pore size of the PC membranes.[29] We obtained 40, 70, and 100 nm diameter nanowires by using PC templates with quoted pore sizes of 10, 30, and 50 nm. Similar features were also observed in commercial anodic alumina membranes and carefully investigated by Xiao et al.[30] They found that the quoted pore size is equal to the pore diameter in the active layer with a small hole. Such a structure is suitable for the application as filters where the small hole in the active layer controls the size of the species that can go through. The diameter of the nanowires grown into the pores of the membranes has a large size controlled by the pore size of the support layer with larger diameter. The situation in PC membrane might have the same origin, where the pore size at one end of the channels is smaller than the inner pore diameter. Freestanding nanowires for TEM imaging were obtained by dissolving the PC membrane in dichloromethane and were stored as a suspension. Transport measurements were carried out on Bi nanowire arrays still embedded in the membrane with a physical properties measurement system (PPMS), equipped with a ^{3}He insert and a superconducting magnet. The schematic arrangement of the system for transport measurement is shown in the inset of Figure 1b, and the details of our technique can be found in refs 31 and 32. The total resistance, R, of the system with this configuration consists of the contributions from the electrodes, the Bi nanowire array, and the interfaces between electrodes and nanowires.

Figure 1a shows the resistance (R) versus temperature (T) of five Bi nanowire samples S1−S5 in the low-temperature regime (T < 10 K), measured at zero magnetic field (H). Curves in the wide temperature range of 0.47−300 K are shown in the inset of Figure 1a. Nanowire samples of 70 nm, S1, S2, and S3, were grown at room temperature at a voltage of −2.3 V, whereas 100 nm diameter samples S4 and S5 were grown at −2.45 V. We selected 0.5 mm diameter superconducting Pb wires (Alfa Aesar, A Johnson Matthey Co.) as the electrodes because Pb is a soft metal and good contact can be easily made by lightly squeezing them onto the two sides of PC membrane. The T_c and zero temperature critical magnetic field (H_c^{Pb}) of Pb electrodes are 7.2 K and 0.94 kOe, respectively. The resistance of the electrodes and the contacts is usually less than 1.0 Ω, much less than that of the Bi nanowires. All five samples show a

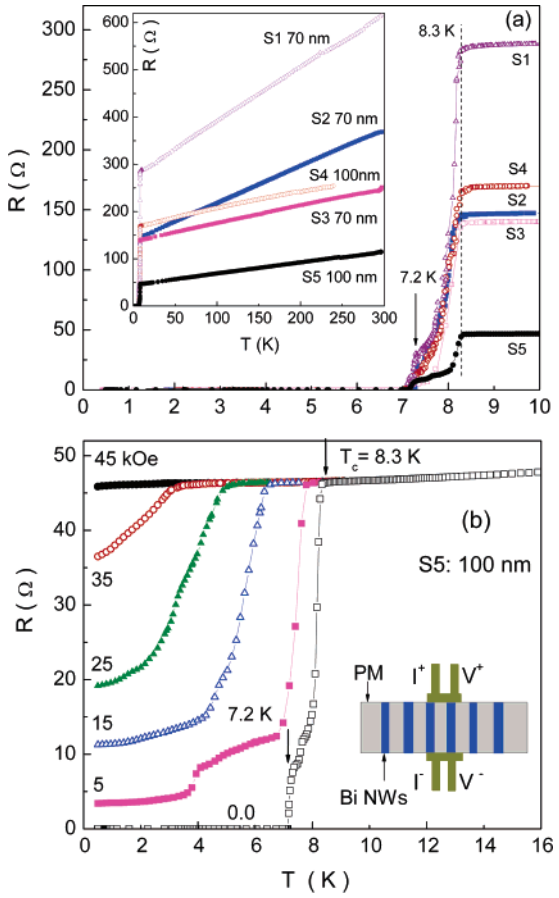

Figure 1. (a) Resistance (R) versus temperatures (T) of several superconducting granular Bi nanowires in low-temperature range: S1−S3, 70 nm; S4 and S5, 100 nm. The inset is the $R-T$ curves in the temperature range of 0.45−300 K under zero magnetic field (H). (b) $R-T$ curves of S5 measured at different H in the low T range; the inset is the schematic arrangement of the transport measurement.

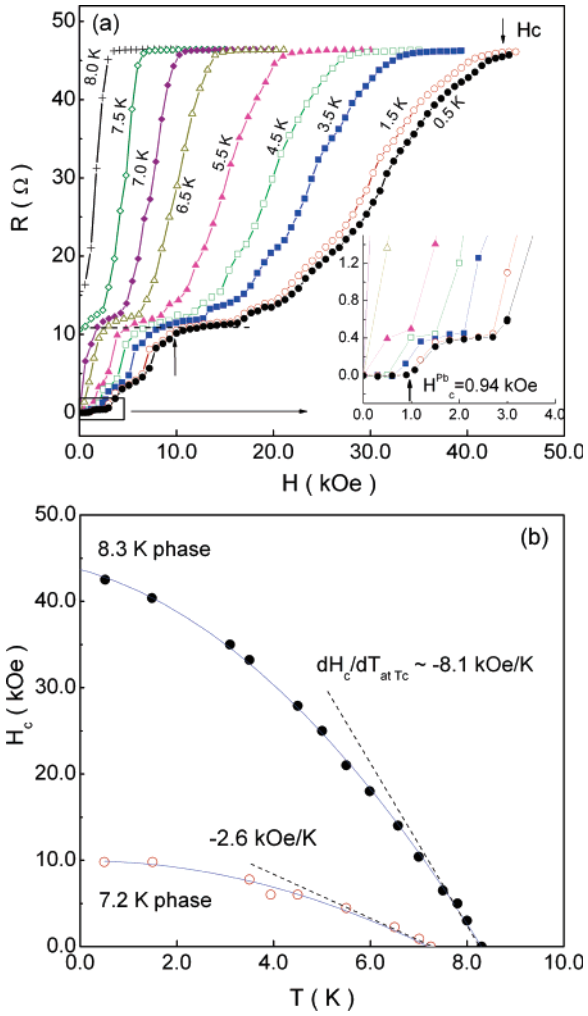

Figure 2. (a) $R-H$ curves of granular nanowires measured at different T; the blow-up plot of the $R-H$ in low field range indicated by the mark is shown in the inset. (b) H_c-T phase diagram of 7.2 and 8.3 K superconducting phases. The solid lines indicate the phase boundaries of the two superconducting phases and are drawn to guide the eye.

sharp, large resistance drop at 8.3 K, followed by a smaller drop around 7.2 K down to zero resistance. The resistance of the samples is linearly dependent on the temperature between 8.3 and 300 K with a residual resistance ratio [RRR = R(300 K)/R(8.3 K)] of 1.7−2.6, indicating that the Bi nanowire samples are metallic above 8.3 K. Assuming that the room-temperature resistivity (ρ_0) of a Bi nanowire is on the order of that of a metallic polycrystalline Bi film, ~11 × 10^{-4} Ω cm,[33] then the number (N) of the Bi nanowires in each nanowire array sample, which make contact with Pb electrodes in our transport measurement, are estimated to be 27, 45, 68, 47, and 70, for samples S1−S5, respectively.

To confirm that the two resistance drops at 7.2 and 8.3 K are related to the superconducting transitions of Bi nanowires, Figure 1b shows the $R-T$ curves of sample S5 ($N \sim 70$) in low-temperature regime, measured at different magnetic fields that were aligned perpendicular to the nanowires. Both T_c values are magnetic field dependent. The T_c of the 8.3 K phase decreases with increasing magnetic field and goes down below 0.47 K at a field of 45 kOe, whereas the T_c of 7.2 K phase disappears at a field between 5.0 and 15 kOe. The large resistance drop at 8.3 K can be unambiguously assigned to a superconducting transition of the Bi nanowires because the transition temperature is higher than the T_c = 7.2 K of the Pb electrodes. The small resistance drop of ~11 Ω at 7.2 K coincides with the T_c of Pb electrodes. Because a small resistance drop at 3.8 K still survives under a magnetic field of H = 5.0 kOe, which is much higher than $H_c^{Pb} \sim 0.94$ kOe, the majority of the 11 Ω drop at 7.2 K is also related to the superconducting transition of the Bi nanowires. Further evidence for this 7.2 K phase will be shown below in the $R-H$ measurements.

Figure 2a shows $R-H$ curves of sample S5 measured at different temperatures. The low field region is magnified in the inset. At T = 0.5 K, the total system is superconducting with R = 0 Ω below the critical field of Pb electrodes (~0.94 kOe). Above 0.94 kOe, resistance jumps to 0.4 Ω and then increases monotonically up to the normal state value of 46 Ω at 45 kOe. The small resistance jump of 0.4 Ω starting at 0.94 kOe is due to the superconducting to normal transition of Pb electrodes. Thus, most of the 11.0 Ω drop in resistance at 7.2 K in the $R-T$ curve (Figure 1b) is not related to the Pb electrodes. In Figure 2a, a significant shoulder at 10 kOe

with a resistance of ~11 Ω is seen and disappears between 7.0 and 7.5 K. Because the applied magnetic field of 10 kOe is much higher than the H_c^{Pb} of the Pb electrodes, we attribute this resistance shoulder to the 7.2 K superconducting phase of the Bi nanowires. If we define the magnetic field indicated by the arrows at the shoulder position as the H_c of the 7.2 K superconducting phase, and the field at which the wires are driven to the normal state as the H_c of the 8.3 K phase, then the $H-T$ phase diagram of the two superconducting phases can be drawn as shown in Figure 2b. According to Ginzburg−Landau−Abrikosov−Gorkov theory[34−36] for a type-II superconductor, the initial slope at T_c of the upper critical field $H_c(T)$ curve determines the electronic density of states $N(E_F)$ at the Fermi surface, i.e., $(dH_c/dT)_{T_c} = -(12e/\pi^3 k_B)\gamma\rho \propto -N(E_F)\rho$, where γ, ρ, k_B, and e are the Sommerfeld constant, normal state residual resistivity, Boltzmann constant, and the electronic charge, respectively. The values, $-(dH_c/dT)_{Tc}$, for 7.2 and 8.3 K superconducting phases in our Bi nanowires were estimated to be 2.6 and 8.1 kOe/K, respectively. These values are noticeably smaller than the values of 20−30 kOe/K for amorphous Bi films[37] and much smaller than 167 kOe/K (or 80 kOe/K) for granular Bi composite films at grain size of 4.2 nm (or grain size larger than 5.0 nm).[28] However, the estimated values in our Bi nanowires lie in the range of 2−15 kOe/K for strong-coupling superconducting films.[37] The differences in the $(dH_c/dT)_{Tc}$ values and the difference in T_c indicate that the two observed superconducting transitions around 7.2 and 8.3 K in Bi nanowire arrays are not related to those found in amorphous Bi film or composite granular film.

The close correspondence of the T_c values on the other hand suggests that the observed superconductivity in our nanowires may arise from the Bi high-pressure phases, Bi−III and −V. In principle, it is possible that some energetically unfavorable bulk phases may be stabilized in nanoscale systems due to their large surface to volume ratio and the large difference in the properties of their surface atoms.[38] Zhang et al.[39] have detected a tiny amount of a metastable high-pressure phase in Bi nanowires confined in porous anodic alumina membranes at room temperature, but there were no transport data to support the observation of this high-pressure phase. Very recently, a face-centered cubic Se high-pressure phase, which in bulk form exists only at $P > 13$ GPa,[18] was also reported in Se nanowires fabricated by electrodepositing Se into porous alumina at ambient pressure.[40]

To look for evidence for the Bi high-pressure phases in these superconducting Bi nanowires, TEM studies were carried out. Figure 3a shows a scanning TEM image of superconducting Bi nanowires (sample S1, $d = 70$ nm). A locally magnified TEM image of a randomly selected wire is shown in Figure 3b. It can be seen that the superconducting Bi nanowires are composed of Bi grains with an average diameter around 10 nm. The granular morphologies along the entire wire and also from wire to wire are uniform. Figure 3a(1) shows the selected area electron diffraction (SAED) pattern taken from the six nanowires highlighted in Figure 3a. The SAED ring pattern can be indexed well to the rhombohedral Bi phase. The data indicate that the majority of granular Bi nanowires are polycrystalline with a bulk rhombohedral Bi structure. In other words, there is no evidence of complex tetragonal Bi−III or bcc Bi−V high-pressure phases. Figure 3b(1) shows a local SAED pattern on a segment of an individual granular wire. In contrast to Figure 3a(1), this local SAED on an individual wire shows

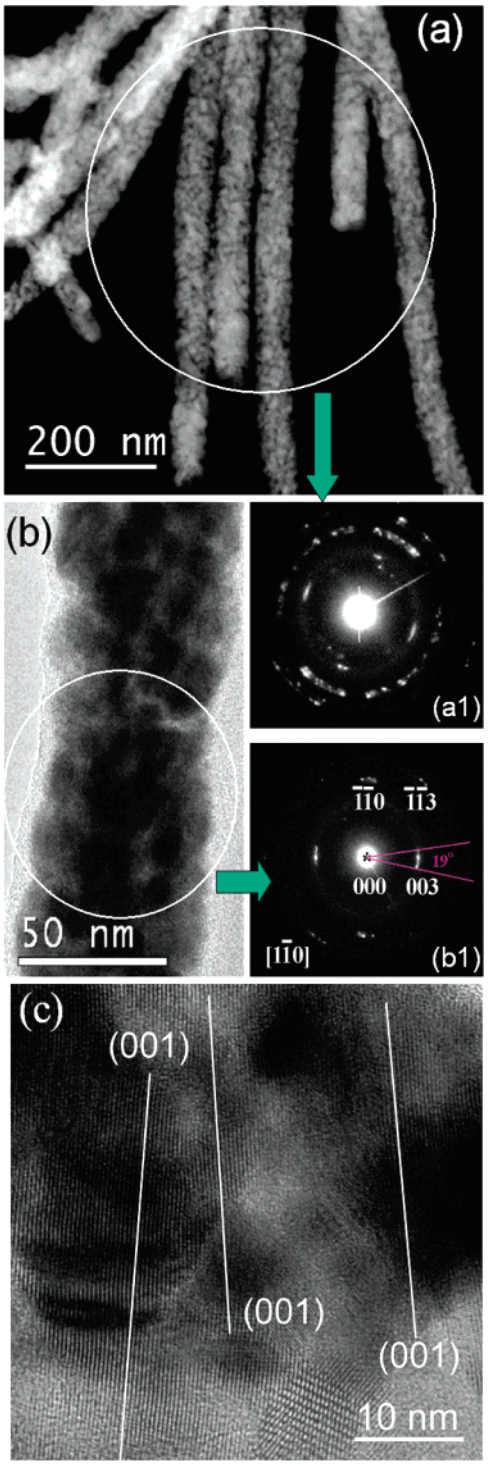

Figure 3. (a) and (a1) are a scanning TEM image of granular Bi nanowires and their SAED pattern, respectively. (b) and (b1) are a magnified TEM image from one part of a ramdomly selected Bi nanowire and its SAED pattern. (c) high-resolution TEM image from Figure 2b.

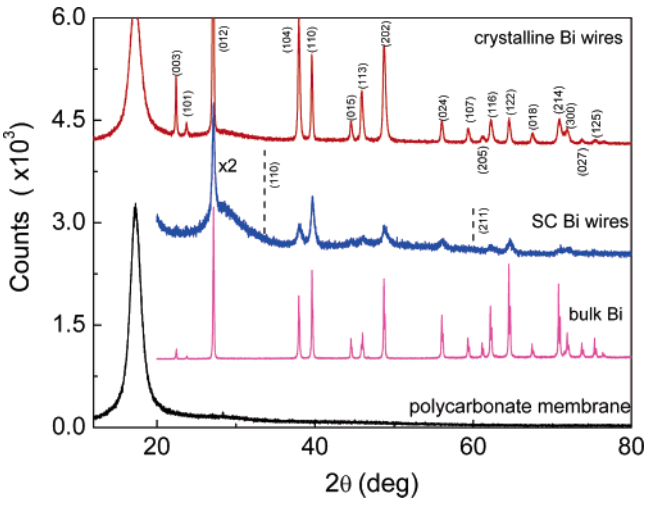

Figure 4. Powder XRD patterns of an empty polycarbonate membrane, bulk Bi powder, superconducting granular Bi nanowires embedded in a polycarbonate membrane, and crystalline Bi nanowires in a membrane, respectively. The curves are shifted up for clarity. The two dashed lines indicate the positions of the two strongest diffraction peak of the bcc high-pressure phase of Bi−V.

"cigar"-like elongated electron diffraction spots, instead of the ring structure. This means that the Bi grains in an individual nanowire are not randomly oriented but have preferred orientations within a small angular distribution. The misorientation of (001) diffraction spots among these grains is within 19° (see Figure 3b(1)). The high-resolution TEM image shown in Figure 3c confirms the (001) orientation of the Bi grains, indicated by the white lines. This interesting texture is the dominant structural feature of all of the granular Bi nanowires that show superconductivity. Our TEM data cannot resolve any structural differences between the wires that show the 7.2 and the 8.3 K transition.

Figure 4 shows X-ray diffraction (XRD) patterns (with Cu KαI radiation) obtained from an empty PC membrane, bulk Bi powder, a superconducting granular Bi nanowire array embedded in a PC membrane (S1), and a crystalline Bi nanowire array embedded in a PC membrane. All the diffraction peaks obtained from granular superconducting Bi nanowires at room temperature can be indexed to the ambient pressure rhombohedral Bi structure. Structural refinement in the $R3m$ space group gives (for the related hexagonal cell) cell parameters, $a = 4.525(5)$ and $c = 11.880(8)$ Å. These values are close to those reported in literature ($a = 4.546$, $b = 11.862$ Å[12]). No additional peaks expected for the bcc Bi−V high-pressure phase, indicated by the dashed lines in the pattern, are seen.[41] The only difference in the superconducting granular Bi wires is that the diffraction peaks become broader, and some of the peaks disappeared when compared with those of bulk Bi powder and non-superconducting crystalline Bi nanowire samples. The broadening and the disappearance of some reflections indicate that the structure of granular Bi nanowires is highly distorted. The broad hump superimposed on the (012) reflection is due to the oxidation of the granular nanowires, which are exposed to air (even if the nanowires are embedded in the template) during the XRD measurement. Hence, the XRD data on superconducting granular Bi nanowires do not show any evidence of high-pressure Bi phases III and V.

One possible explanation on the apparent discrepancy between the transport measurements and structural data is that the nanowires that show a rhombohedral structure at room temperature may transform into high-pressure phases at low temperatures due to the differential thermal contraction between PC membrane and the wires during cooling. If this were the case, however, one would expect some features in the $R-T$ curves to appear at some intermediate temperatures when the structural transition takes place. The inset of Figure 1 shows metallic behavior for all our superconducting Bi nanowires, and the linear $R-T$ curves extended from room temperature down to 8.3 K without a discontinuous resistance change or a change in slope. It is extremely unlikely that the structural transformation to the Bi−III and −V phases takes place exactly at their superconducting transition temperatures 7.2 and 8.3 K.

Another possible explanation is that there are no high-pressure phases in granular superconducting Bi nanowires, but the rhombohedral Bi grains themselves are superconducting with T_c values of 7.2 K or 8.3 K due to quantum confinement effects. If this were the case, superconductivity would be expected in any granular Bi films or wires with similar grain size. However, granular Bi films and wires with grain sizes of 10−20 nm, fabricated by dc sputtering Bi onto cooled substrates,[9] are not superconducting. It would also be a very unusual coincidence if the observed T_c values coincided precisely with the T_c values of the Bi high-pressure phases III and V, neither of which is rhombohedral.

Figure 5a shows the TEM image of a 70 nm Bi nanowire sample (S6) deposited at −2.45 V. This sample shows a granular morphology, but the grain size is not uniform from wire to wire and even between different segments of the same wire. Locally magnified images of the marked areas of the wires are shown in parts b and c of Figure 5, where the grain size of the wires ranges between 6 and 8 nm. It is noted that the diameter of the nanowire shows a significant change at the junctions between two segments with different morphology; i.e., the segments with large grains show a relatively large diameter, while the segments with small grains show a small diameter (see parts a and d of Figure 5). We do not know why the wire diameter closely depends on the wire morphology, but the wire diameter of Bi nanowires was found to be adjustable by changing the deposition parameter (such as, using electric pulse) and can be much smaller than the pore size.[42] Here we use dc voltage to grow Bi nanowires, which is different from the case in ref 42. The significant change of the diameter between two segments of the wire with different morphology still remains unclear and worth investigating in the future. However, the variations of the wire morphology from segments to segments are considered to be from the fluctuations of the growth rate during the deposition. This nonuniform morphology of the nanowires is in contrast to the uniform granular morphology shown in parts a and b of Figure 3. The $R-T$ curves measured on this sample at a magnetic field of $H = 0$, 30, 50, and 80 kOe with an excitation current of 10 nA are shown in Figure 6a.

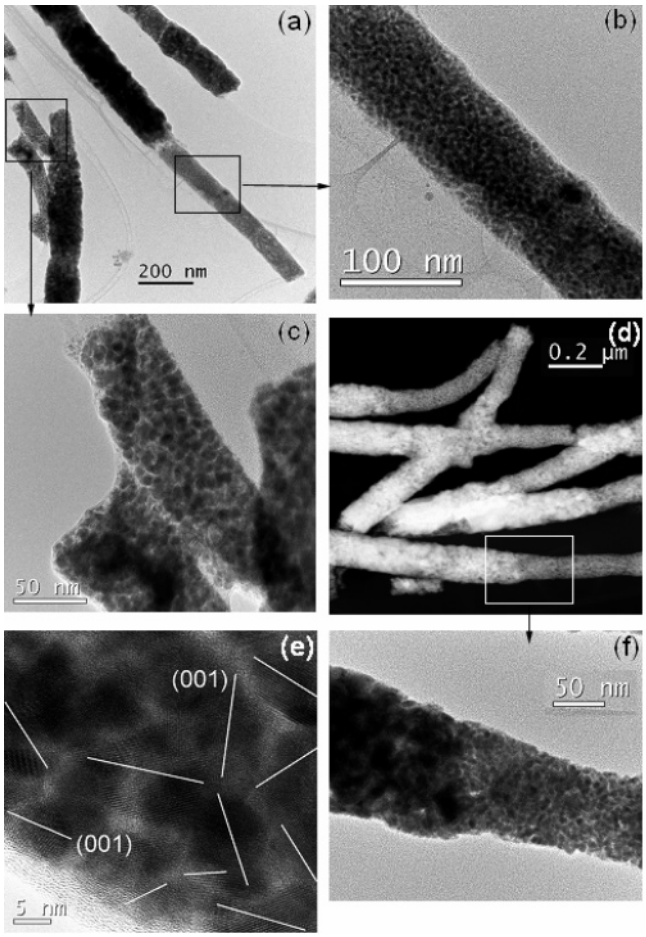

Figure 5. (a) Low magnification TEM image of non-superconducting granular Bi nanowires S6, deposited at $V = -2.3$ V. (b) and (c) are the magnified TEM images from the marked area shown in (a). (d) Low magnification STEM image of non-superconducting granular Bi nanowires S7, deposited at $V = -2.45$ V. (e) Local HRTEM image of (c) showing random orientation of the grains. (f) The magnified TEM image from the marked area shown in (d).

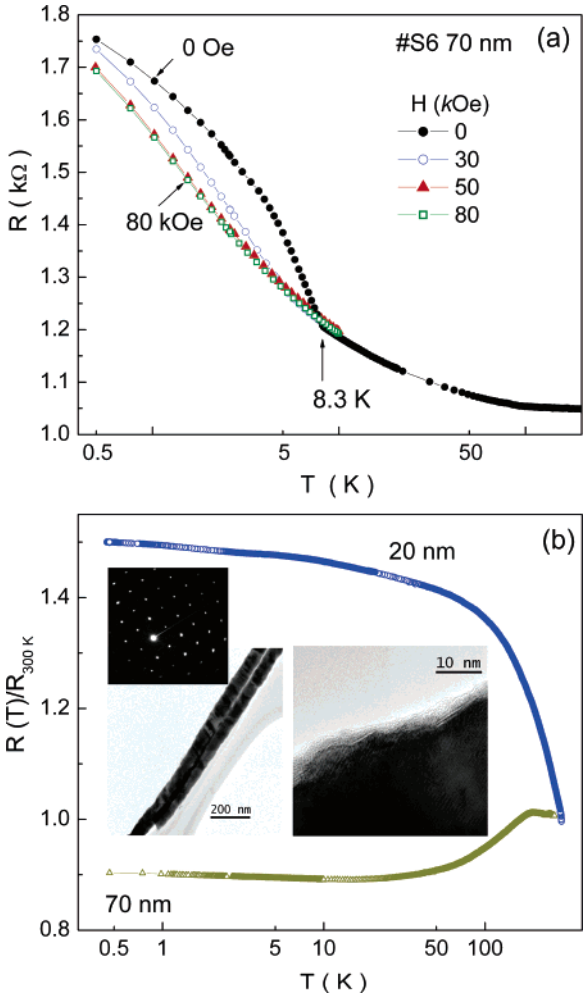

Figure 6. (a) $R-T$ curves of granular Bi nanowires (S6), measured at different magnetic fields. A superresistive state below 8.3 K is observed at $H = 0$ Oe. (b) $R-T$ curves of single-crystalline Bi nanowires S8 (20 nm) and S9 (70 nm) measured at $H = 0$ Oe. The insets are the TEM image, high-resolution TEM image, and electron diffraction pattern of 70 nm diameter single-crystalline Bi nanowires.

This granular sample S6 exhibits semiconducting behavior from 300 down to 8.3 K. An unusual enhancement of resistance below 8.3 K is seen under zero magnetic field. Interestingly, the "extra resistance" below 8.3 K decreases with increasing magnetic field. When the magnetic field is larger than 50 kOe, this superresistive state below 8.3 K is completely suppressed and thus the $R-T$ curves show a smooth semiconducting behavior down to 0.5 K insensitive to further increase in magnetic field. The possible mechanism for this "superresistive" state will be discussed below. These comparative studies rule out the possibility that the superconductivity in the granular Bi nanowires originates from the quantum size effect of rhombohedral Bi grains.

Figure 5e shows a high-resolution TEM image of a small local region of the wire shown in Figure 5c. In contrast to the textured grains shown in Figure 3c, the Bi grains in these non-superconducting granular wires are entirely randomly oriented. This is a common feature for all non-superconducting granular wires. Figure 5d shows the STEM image of another non-superconducting Bi nanowire (S7), deposited at a more negative voltage, −3.0 V. This image is similar to that shown in Figure 5a showing highly nonuniform granular morphology. A locally enlarged TEM image of the marked area is shown in Figure 5f. Most of the nanowires consist of fine grains that are 5−7 nm in diameter. These results allow us to speculate that the superconducting high-pressure phase in Bi nanowires probably arises from the grain boundary areas, and its appearance or disappearance depends not only on the granular morphology but also on how these grains are oriented and joined together. In other words, the formation of superconducting high-pressure phases at grain boundaries requires a certain degree of orientational order between the neighboring grains. On the other hand, if there is a perfect orientation order and the nanowire becomes a single crystal, the nanowires are never superconducting. Figure 6b shows the $R-T$ curves of the 70 nm (S8) and 20 nm (S9) diameter single-crystalline Bi nanowires (S9 is fabricated with homemade anodic aluminum oxide templates).[43] These wires were deposited at a voltage of −2.0 V without the additive chemicals NaCl and K_2SO_4. TEM images are shown in the inset of Figure 6b. Sample S8 (70 nm) shows metallic behavior from 200 to 20 K. Below 20

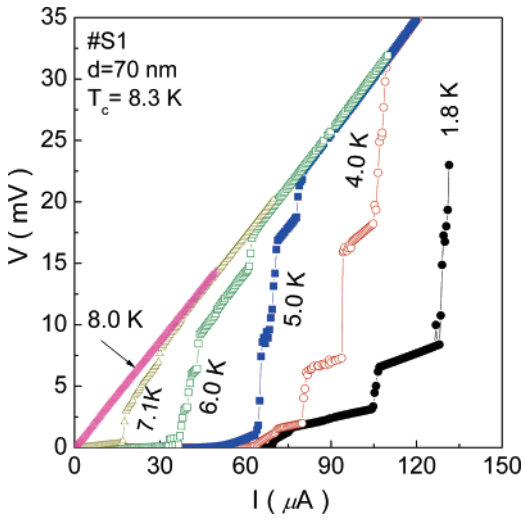

Figure 7. *V*−*I* characteristics of superconducting granular Bi nanowires (sample S1), measured at different temperatures.

K, its resistance shows a slight increase with decreasing temperature down to 0.47 K. Sample S9 (20 nm) shows semiconducting behavior from room temperature down to 0.47 K. These data on crystalline Bi nanowire arrays are consistent with previous reports.[6] The metallic to semiconducting transition of crystalline Bi nanowires with decreasing wire diameter (~60 nm) has been attributed to a size confinement effect on the electronic band structure.[7]

We propose the following hypothesis to explain all the observed experimental results. We propose that the observed superconducting transition is due to small amounts of high-pressure phases B−III and −V stabilized between rhombohedral grains. In the textured granular wires where the grains are aligned throughout the length of the wires, the high-pressure Bi phase forms continuous paths resulting in the superconductivity of these wires. Since the fractions of the high-pressure phases are minute, they escaped detection by TEM and XRD in the presence of the majority rhombohedral phase. It is also possible that the high-pressure phase at the grain boundaries may be oxidized when the Bi nanowires are exposed to air for TEM or XRD measurements.

To test this hypothesis, we measured the critical currents of the superconducting Bi nanowires. Figure 7 shows *V*−*I* curves of sample S1 ($d = 70$ nm, $T_c = 8.3$ K), measured at different temperatures $T < T_c$. These curves show a few sharp voltage steps in approaching the normal state. If we define the current value at the initial point of the first voltage step as the critical current I_c, then the critical current density, j_c, of an individual superconducting granular Bi nanowire can be estimated by the formula $j_c = (I_c R_0/\rho_0 L)(S_0/S_{eff})$, where I_c, R_0, ρ_0, and L are the critical current, room-temperature resistance, room-temperature resistivity, and the length of the Bi nanowire, respectively. S_0 is the cross-sectional area of an individual Bi nanowire and S_{eff}/S_0 the fraction of the cross section that is superconducting. We make the assumption that the ratio, S_{eff}/S_0, in each nanowire in the array is the same due to the uniformity of the nanowire morphology. If we take $\rho_0 \sim 11 \times 10^{-4}$ Ω cm for a polycrystalline Bi film,[36] we get $j_c = 6.5 \times 10^4$ (S_0/S_{eff}) A/cm^2 for 70 nm granular Bi nanowires ($I_c = 68$ μA at 1.8 K, $R_0 = 620$ Ω, and $L = 6$ μm). For 100 nm Bi nanowires (sample S5), j_c is found to be 6.4×10^4 (S_0/S_{eff}) A/cm^2 ($I_c = 350$ μA at 1.8 K, $R_0 = 120$ Ω, and $L = 6$ μm). The critical current densities for a number of superconducting nanowires around 1.8 K are reported to be 5.5×10^6 A/cm^2 for Pb nanowires,[44] 0.9×10^6 to 1.7×10^6 A/cm^2 for Sn nanowires,[32,44] 4.5×10^6 A/cm^2 for In nanowires,[45] and 10×10^6 A/cm^2 for Nb nanowires.[46] Because the Nb and Pb nanowires have a comparable higher T_c with our granular Bi nanowires, it is reasonable to assume that the j_c of the superconducting channels in Bi nanowires should be on the same order of $(5.5-10.0) \times 10^6$ A/cm^2. On the other hand, Nb nanowires[46] shows a very similar granular morphology with grain size of a few nanometers, while the Pb nanowires[44] were grown by a similar electrodeposition technique. Such an assumption yields a value of S_{eff}/S_0 for the Bi granular nanowire to be 0.01. These results suggest that only about 1.0% of the cross-sectional area of an individual wire is superconducting. This is consistent with the model of small amounts of superconducting high-pressure phases survived at grain boundary areas. If we model the superconducting channels between the 10 nm crystalline rhombohedral grains as "filaments" through the whole wire, then the thickness of the superconducting filaments will be on the order of 1.0 nm. Such a small size of superconducting high-pressure phases is difficult to be recognized by TEM image and XRD, even if the high-pressure phases at grain boundary areas were not oxidized.

The sharp voltage steps observed in the *V*−*I* curves (Figure 7) are very similar to those found in quasi-one-dimensional superconducting nanowires or whiskers.[47−50] Usually, these voltage steps in quasi-one-dimensional (1D) superconduting wires have been interpreted to be a consequence of spatially localized "weak spots" or phase-slip centers[51−53] due to the inhomogeneity of the wire. In Bi nanowire arrays, the 1.0 nm superconducting filaments are probably equivalent to a 1D superconductor; the similar voltage steps in *V*−*I* curves might have the similar mechanism related to the phase-slip centers.

Our model can also explain why the superconductivity in granular Bi nanowires is very subtle and sample dependent. Although the granular Bi nanowires can be electrochemically deposited at a voltage between −2.2 and −3.0 V, the orientation of the grains and the uniformity from wire to wire are hard to control. However, in the non-superconducting nanowires, we do not exclude the possibility that some local superconducting clusters survive because the Bi grains may locally show a preferred orientation. These local areas thus fit the requirement for the formation of superconducting high-pressure phase but do not form a continuous superconducting channel through the length of the wire. The observed superresistive state below 8.3 K at $H = 0$ Oe shown in Figure 6 may be the consequence of local superconducting clusters separated by semiconducting (Sm) grains in the wire. This case is similar to a percolation superconductor in a random system,[54,55] where the fraction of superconducting phase is below the percolation threshold. The conductivity of the system (S−Sm−S) below T_c is then dominated by single-

electron quasi-particle tunneling between the superconducting clusters. When an applied magnetic field reduces the energy gap of superconducting clusters to zero, the resistivity of the system is reduced to that corresponding to a N−Sm−N system. This corresponds to the case shown in Figure 6a, where the $R-T$ curve at $H > 50$ kOe is below the one at $H = 0$ Oe and shows smooth semiconducting behavior down to 0.47 K.

In summary, granular Bi nanowires composed of well-defined ~10 nm diameter rhombohedral Bi grains were fabricated by electrochemically depositing Bi into porous membranes. Transport measurement showed that the granular Bi nanowires exhibit superconductivity at 7.2 and 8.3 K, and these T_c values coincide with superconducting transition temperatures of the high-pressure phases of Bi−III and −V. We believe that the superconductivity of granular Bi nanowires is from grain boundary areas due to structural reconstruction and not from the rhombohedral Bi grains. Further experimental and theoretical investigations may be very helpful in shedding more light on the origin of supercondcutivity in granular Bi nanowires.

Acknowledgment. We thank Dr. Vincent Crespi and Dr. Ning Wang for fruitful discussions. This work is supported by Penn State MRSEC funded by NSF under Grant DMR-0213623.

References

(1) Kurti, N.; Simon, F. E. *Proc. R. Soc. London, Ser. A* **1935**, *151*, 610.
(2) Overcash, D. R.; Ratnam, B. A.; Skove, M. J.; Stillwell, E. P. *Phys. Rev. Lett.* **1980**, *44*, 1348.
(3) Hoffman, R. A.; Frankl, D. R. *Phys. Rev. B* **1971**, *3*, 1825.
(4) Yang, F. Y.; Liu, K.; Hong, K. M.; Reich, D. H.; Searson, P. C.; Chien, C. L. *Science* **1999**, *284*, 1335.
(5) Brandt, N. B.; Gitsu, D. V.; Nikolaeva, A. A.; Ponomarev, Ya. G. *Sov. Phys. JETP* **1977**, *45*, 1226. Brandt, N. B.; Gitsu, D. V.; Dolma, V. A.; Ponomarev, Y. G. *Sov. Phys. JETP* **1987**, *65*, 515.
(6) Heremans, J.; Thrush, C. M.; Lin, Y. M.; Cronin, S.; Zhang, Z.; Dresselhaus, M. S.; Mansfield, J. F. *Phys. Rev. B* **2000**, *61*, 2921. Heremans, J.; Thrush, C. M.; Zhang, Z.; Sun, X.; Dresselhaus, M. S.; Ying, J. Y.; Morelli, D. T. *Phys. Rev. B* **1998**, *58*, 10091.
(7) Zhang, Z. B.; Sun, X. Z.; Dresselhaus, M. S.; Ying J. Y.; Heremans, J. *Phys. Rev. B* **2000**, *61*, 4850. Lin, Y. M.; Sun, X.; Dresselhaus, M. S. *Phys. Rev. B* **2000**, *62*, 4610.
(8) Liu, K; Chien, C. L; Searson, P. C.; Zhang, K. Y. *Appl. Phys. Lett.* **1998**, *73*, 1436.
(9) Beutler, D. E.; Giordano, N. *Phys. Rev. B* **1988**, *38*, 8.
(10) Nikolaeva, A.; Gitsu, D.; Huber, T.; Konopko, L. *Physica B* **2004**, *346−347*, 282.
(11) Li, L.; Yang, Y. W.; Huang, X. H.; Li, G. H.; Ang, R.; Zhang, L. D. *Appl. Phys. Lett.* **2006**, *88*, 103119.
(12) Degtyareva, O.; McMahon, M. I.; Nelmes, R. J. *High Pressure Res.* **2004**, *24*, 319.
(13) Nedellec, P.; Dumoulin, L.; Noer, R. J. *J. Phys. F*: *Metal Phys*. **1974**, *4*, L145. Brugger, R. M.; Bennion, R. B.; Worlton, T. G. *Phys. Lett. A* **1967**, *24A*, 714.
(14) Degtyareva, O.; McMahon, M. I.; Nelmes, R. J. *Mater. Sci. Forum* **2001**, *378−381*, 469.
(15) Haussermann, U.; Soderberg, K.; Norrestam, R. *J. Am. Chem. Soc.* **2002**, *124*, 15359.
(16) Imasaki, H.; Chen, J. H.; Kikegawa, T. *Rev. Sci. Instrum.* **1995**, *66*, 1388.
(17) Chen, T. T.; Chen, J. T.; Leslie, J. D.; Smith, H. J. T. *Phys. Rev. Lett.* **1969**, *22*, 526.
(18) Brandt, B.; Ginzburg, N. I. *Sov. Phys. JETP* **1961**, *12*, 1082. Brandt, B.; Ginzburg, N. I. *Sov. Phys. JETP* **1963**, *17*, 326.
(19) Stromberg, H. D.; Stephens, D. R. *J. Phys. Chem. Solids* **1964**, *25*, 1015.
(20) Brandt, N. B.; Ginzburg, N. I. *Comtemp. Phys.* **1969**, *10*, 355.
(21) Wittig, J. *Z. Phys.* **1966**, *195*, 215.
(22) Buckel, W.; Wittig, J. *Phys. Lett.* **1965**, *17*, 187.
(23) Weitzel, B.; Micklitz, H. *Phys. Rev. Lett.* **1991**, *66*, 385.
(24) Weitzel, B.; Schreyer, A.; Micklitz, H. *Europhys. Lett.* **1990**, *12*, 123.
(25) Vossloh, C.; Holdenried, M.; Micklitz, H. *Phys. Rev. B.* **1998**, *58*, 12422.
(26) Moodera, J. S.; Meservey, R. *Phys. Rev. B* **1990**, *42*, 179.
(27) LeClair, P.; Moodera, J. S.; Philip, J.; Heiman, D. *Phys. Rev. Lett.* **2005**, *94*, 037006.
(28) Van Hulst, J. A.; Rietveld, G.; Van der Marel, D.; Tuinstra, F.; Jaeger, H. M. *Phys. Rev. B* **1993**, *47*, 548. Moodera, J. S.; Meservey, R. *Phys. Rev. B* **1993**, *47*, 550.
(29) Tian, M. L.; Wang, J. G.; Kurtz, J.; Mallouk, T. E.; Chan, M. H. W. *Nano Lett.* **2003**, *3*, 919. Tian, M. L.; Wang, J. G.; Snyder, J.; Kurtz, J.; Liu, Y.; Schiffer, P.; Mallouk, T. E.; Chan, M. H. W. *Appl. Phys. Lett.* **2003**, *83*, 1620.
(30) Xiao, Z. L.; Han, C. Y.; Welp, U.; Wang, H. H.; Kwok, W. K.; Willing, G. A.; Hiller, J. M.; Cook, R. E.; Miller, D. J.; Crabtree, G. W. *Nano Lett.* **2002**, *2*, 1293.
(31) Tian, M. L.; Kumar, N.; Xu, S. Y.; Wang, J. G.; Kurtz, J. S.; Chan, M. H. W. *Phys. Rev. Lett.* **2005**, *95*, 076802.
(32) Tian, M. L.; Wang, J. G.; Kurtz, J. S.; Liu, Y.; Chan, M. H. W.; Mayer, T. S.; Mallouk, T. E. *Phys. Rev. B* **2005**, *71*, 104521.
(33) Huber, T. E.; Celestine, K.; Graf, M. J. *Phys. Rev. B* **2003**, *67*, 245317.
(34) Ginzburg, V. L.; Landau, L. D. *Zh. Eksp. Teor. Fiz.* **1950**, *20*, 1064.
(35) Abrikosov, A. A. *Zh. Eksp. Teor. Fiz.* **1957**, *32*, 1442 [*Sov. Phys. JETP* **1957**, *5*, 1174].
(36) Gorkov, L. P. *Zh. Eksp. Teor. Fiz*. **1958**, *34*, 735 [*Sov. Phys. JETP* **1958**, *7*, 505]; *Zh. Eksp. Teor. Fiz.* **1959**, *36*, 1918 [*Sov. Phys. JETP* **1959**, *9*, 1364].
(37) Bergmann, G. *Phys. Rev.* **1973**, *7*, 4850. Lazarev, G. G.; Lazareva, L. S.; Semeneko, E. E.; Tutov, V. I.; Goridov, S. I. *Sov. Phys*. **1971**, *16*, 147.
(38) Wang, Z. L.; Gao, R. P.; Nikoobakht, B.; El-Sayed, M. A. *J. Phys. Chem. B* **2000**, *104*, 5417.
(39) Zhang, Z. B.; Gekhtman, D.; Dresselhaus, M. S.; Ying, J. Y. *Chem. Mater*. **1999**, *11*, 1659.
(40) Zhang, X. Y.; Cai, Y.; Miao, J. Y.; Ng, K. Y.; Chan, Y. F.; Zhang, X. X.; Wang, N. *J. Cryst. Growth* **2005**, *276*, 674.
(41) Schaufelfelberger, P. *High Temp. High Pressure* **1973**, *5*, 221.
(42) Li, L.; Zhang, Y.; Li, G.; Zhang, L. D. *Chem. Phys. Lett.* **2003**, *378*, 244.
(43) Tian, M. L.; Xu, S. Y.; Wang, J. G.; Kumar, N.; Wertz, E.; Li, Q.; Campbell, P. M.; Chan, M. H. W.; Mallouk, T. E. *Nano Lett.* **2005**, *5*, 967.
(44) Michotte, S.; Matefi-Tempfli, S.; Piraux, L. *Appl. Phys. Lett.* **2003**, *82*, 4119.
(45) Giordano, N. *Phys. Rev. B* **1990**, *41*, 6350.
(46) Rogachev, A.; Bezryadin, A. *Appl. Phys. Lett.* **2003**, *83*, 512.
(47) Schulz, U.; Tidecks, R. J. *Low Temp. Phys*. **1988**, *71*, 151. Schulz, U.; Tidecks, R. J. *Solid State Commun*. **1986**, *57*, 29.
(48) Slama, G.; Tidecks, R. *Solid State Commun.* **1982**, *44*, 425.
(49) Werner, T.; Tidecks, R.; and Johnston, B. D. *J. Cryst. Growth* **1985**, *73*, 467.
(50) Meyer, J.; and Minnigerode, G. V. *Phys. Lett*. **1972**, *38A*, 529.
(51) Kadin, A. M.; Skocpol, W. J.; Tinkham, M. *J. Low Temp. Phys.* **1978**, *33*, 48.
(52) Skocpol, W. J.; Beasley, M. R.; Tinkham, T. *J. Low Temp. Phys.* **1974**, *16*, 1456.
(53) Michotte, S.; Matefi-Tempfli, S.; Piraux, L.; Vodolazov, D. Y.; Peeters, F. M. *Phys. Rev. B* **2004**, *69*, 094512.
(54) Geiber, A.; Deutscher, G. *Phys. Rev. B* **1987**, *35*, 3214. Geiber, A.; Deutscher, G. *Phys. Rev. Lett.* **1989**, *63*, 1184.
(55) Wu, W. H.; Adam, P. W. *Phys. Rev. B* **1994**, *50*, 13065.

NL0618041